OPEN ACCESS
IOP Publishing
Nanotechnology

Nanotechnology **27** (2016) 095702 (14pp)
doi:10.1088/0957-4484/27/9/095702

Screen-printed nanoparticles as anti-counterfeiting tags

Carlos Campos-Cuerva[1,2,5], Maciej Zieba[1,2,5], Victor Sebastian[1,2], Gema Martínez[1,2], Javier Sese[1,3], Silvia Irusta[1,2], Vicente Contamina[4], Manuel Arruebo[1,2] and Jesus Santamaria[1,2]

[1] Institute of Nanoscience of Aragon (INA) and Department of Chemical Engineering and Environmental Technology, University of Zaragoza, C/Mariano Esquillor, s/n, I + D + i Building, 50018, Zaragoza, Spain
[2] CIBER de Bioingeniería, Biomateriales y Nanomedicina (CIBER-BBN), Centro de Investigación Biomédica en Red. C/Monforte de Lemos 3-5, Pabellón 11, 28029 Madrid, Spain
[3] Departamento de Física de la Materia Condensada, University of Zaragoza, 50009 Zaragoza, Spain
[4] Tipolinea S.A.U., Calle Isla de Mallorca, 13, 50014 Zaragoza, Spain

E-mail: arruebom@unizar.es and jesus.santamaria@unizar.es

Received 30 October 2015, revised 10 December 2015
Accepted for publication 7 January 2016
Published 29 January 2016

Abstract

Metallic nanoparticles with different physical properties have been screen printed as authentication tags on different types of paper. Gold and silver nanoparticles show unique optical signatures, including sharp emission bandwidths and long lifetimes of the printed label, even under accelerated weathering conditions. Magnetic nanoparticles show distinct physical signals that depend on the size of the nanoparticle itself. They were also screen printed on different substrates and their magnetic signals read out using a magnetic pattern recognition sensor and a vibrating sample magnetometer. The novelty of our work lies in the demonstration that the combination of nanomaterials with optical and magnetic properties on the same printed support is possible, and the resulting combined signals can be used to obtain a user-configurable label, providing a high degree of security in anti-counterfeiting applications using simple commercially-available sensors.

Keywords: anti-counterfeiting, nanoparticles, screen printing, serigraphy, magnetic, plasmonic, aging.

(Some figures may appear in colour only in the online journal)

1. Introduction

According to the International Chamber of Commerce the impact of counterfeiting is estimated at 5%–7% of world trade, worth an estimated $600 billion a year [1]. In addition to other well-established anti-counterfeiting technologies, nanoparticles and nanostructured surfaces are being actively studied as materials able to provide new protective measures. A variety of reasons justify this effort. First, the strong correlation between the nanoparticle properties and their physical and chemical characteristics (nature, size, shape, surface functionalization) implies that these properties are inherently difficult to replicate unless a highly precise fabrication method is used to produce nanoparticles narrowly tuned to the desired property range. Second, because of this dependence, the characterization of the synthesized nanomaterials used as labels or tags, becomes a key step to ensure that they have the desired characteristics. However, characterization generally involves the use of sophisticated equipment including high-resolution electron microscopes, surface analyzers capable of focussing a few nanometers in depth (x-ray photoelectron

[5] These authors contributed equally to this work.

spectroscopy, XPS), atomic analyzers, confocal fluorescence or Raman microscopes and crystalline structure identification systems (EDX, XRD or electron diffraction). These instruments are expensive and require highly specialized personnel, further hampering the process of counterfeiting. Finally, working at the nanoscale makes the nanostructured materials useful as covert (invisible) taggants because the size of those materials is far below the limit of the optical resolution of the human eye at a comfortable viewing distance (~100 micron).

A wide variety of nanomaterials have been used for anti-counterfeiting purposes. Up-conversion nanoparticles stand out as optical labels due to their inherent absorption of two or three higher wavelength photons to give tunable emissions in the visible to ultraviolet range depending on the rare earth added [2]. Serigraphy [3] and ink jet printing [4] have been used to protect paper-based substrates using up-conversion nanoparticles in combination with down-conversion inks. QR codes have been printed as such or as synthetic opals, and alternative readout systems have been implemented using smart phones [5, 6]. Even multicolor nanotaggants based on lanthanide-doped up-converting nanoparticles are possible thanks to epitaxial growth of different phases on the same crystal [7].

Ink-jet printed carbon dots [8] and quantum dots [9] are also interesting labels due to their broad absorption and narrow band emission that can be tuned based on their composition and size. Anisotropic nanoparticles are also used in forgery prevention due to their specific size-dependent properties such as transverse and longitudinal modes of surface plasmon oscillations in the case of gold nanorods [10], dual-mode emissions in the case of up-converting nanoparticles [11] and surface-enhanced Raman scattering properties [12]. In this regard, silver nanowires are capable of polarization-dependent surface-enhanced Raman scattering and, using this technology, covert signatures of the dyes are revealed only depending on the polarization of the incident light [13]. These plasmonic SERS labels can be mixed and matched with different geometrical structures and probe molecules, making such security labels extremely difficult to forge. Giant Raman scattering effects have been demonstrated using encapsulated and aggregated dye molecules inside carbon nanotubes allowing the realization of a library of nanoprobe labels for Raman with robust detection using multispectral analysis [14]. Security data encryption has also been demonstrated with core–shell particles that use different dyes in the core and in the shell to produce a multidye nanostructured material that allows storage of different data on a single spot [15].

Plasmonic nanoparticles have been used to create holograms with properties that go beyond the normal limits of diffraction [16]. Nanocomposites exploit the properties of the constituent materials and therefore present many possibilities in anti-counterfeiting applications. Thus, high contrast holograms can be produced when the nanoparticles used as fillers are periodically assembled within photopolymers [17], electrochromic nanocomposites produce covert or overt signals depending on the electrical current applied [18] and layer-by-layer structures containing nanopillar arrays prepared by photolithography can be engineered to reveal covert or overt patterns [19]. Finally, one-dimensional photonic crystals based on alumina have been fabricated with induced planar defects to make them visible under infrared light but invisible when using natural light [20].

Besides the above described optical signaling nanostructured materials, magnetic nanoparticles are also used as tags to provide characteristic magnetic signatures in different patterns that are easily readable with commercially-available giant magnetoresistive sensors. Their use as anti-counterfeiting signatures able to be deposited using ink jet printers was postulated more than ten years ago [21]. Magnetic nanoparticles compared to microparticles provide the great benefit of being superparamagnetic (no remanence or coercive field) upon exposure to a magnetic field, and invisible as colloidal formulations. They can also be combined with other nanoparticles to produce dual magneto-optical signals. In this regard, magnetic alignment combined with the arrangement as photonic crystals allows forming optical logos with multiple axially symmetric orientations [22]. Depending on the size of the magnetic nanoparticles their response to an externally applied magnetic field can be used to align them independently forming photonic band-gap hetero-structures with different colors [23]. Also, magnetic recovery has been used to concentrate magnetic nanoparticles functionalized with DNA added as taggants in oils to prevent oil falsification and allow unique identification signatures [24]. Other nano-based structures to fight forgery include covert barcodes that exploit metallic and organic nanoparticles capable of well-defined phase changes [25].

It seems obvious that combining nanoparticles capable of different responses could make even more difficult the possibility of replication by counterfeiters. For example, the characteristic extinction spectrum of gold nanoparticles can be blue shifted by depositing a shell of another metal (silver) on the surface providing unique identification characteristics [26]. Also the random disposition of silver nanowires coated with fluorescent dyes after deposition on a support is very difficult to replicate but easy to authenticate just by using fluorescence microscopy [27]. Nanocomposites based on nanosized cellulose fibrils and up-converting nanoparticles combine the strong up-conversion luminescence of lanthanide-doped materials with the transparency, good mechanical stability and flexibility provided by the cellulose [28]. Not only the nanoparticles themselves but also their surface functional groups can contribute to efficient signatures to prevent forgery. In this regard, Creran *et al* [29] reported the use of surface ligands with unique structures and mass fingerprints as 'mass barcodes' to identify gold nanoparticles by using laser desorption/ionization imaging mass spectrometry.

Industry has rapidly grasped the potential of nanomaterials in this field and several companies nowadays commercialize nano-based technologies to win back control of their products and ward off falsifications. Of special interest are those instances where falsification may give rise to health problems, like in products of the pharmaceutical industry. Authentix Inc., Scriba Nanotecnologie, Ingenia Technology, Oxonica Ltd, Attophotonics Biosciences GmbH, Celanese Corp., NanoTech Security Corp., Sun Innovations Inc.,

NanoBright Technologies Pvt Ltd, Evident Technologies are examples of companies offering different nano-solutions to fight against fraud. In spite of this effort, a wide-ranging nanomaterials-based authentication method is not yet available. This is in part due to practical problems regarding the formulation of inks containing different nanomaterials, their adaptation to the printing technique used and the interaction of the nanomaterials with the support (paper, textiles) to be authenticated. Other aspects of concern are the reproducibility of the labels and their aging behavior.

In this work, we have explored the possibility of obtaining advanced anti-counterfeiting capabilities by using a relatively simple method, susceptible of industrial application and we have paid special attention to the above discussed practical problems. We have chosen single-phase, spherical nanoparticles without (or with minimal) functionalization (gold, silver and magnetite) and applied them on different paper supports by a standard screen printing method. The combination of these nanoparticles can therefore provide optical and magnetic signals on the same tagging act, i.e., multiple tags can be screen printed on the same spot, and their responses can be independently detected. Other aspects relevant to potential application such as the influence of the paper support and the ability of the labels to withstand accelerate weathering conditions after tagging have also been studied.

2. Experimental details

2.1. Materials

All chemicals were purchased from Sigma Aldrich and used as received including silver nitrate ($AgNO_3$, 99.9999% trace metals basis), polyvinylpyrrolidone (PVP, Mw = 10 000 Da), ethylene glycol (EG, anhydrous, 99.8%), triethylene glycol (TEG, anhydrous 99%), Iron(III) acetylacetonate (⩾97%), sodium borohydride ($NaBH_4$, ⩾99%), chloroauric acid trihydrate ($HAuCl_4 \cdot 3H_2O$, 99.99%), L-ascorbic acid (99%), sodium hydroxide (reagent grade, ⩾98%), hexadecyltrimethylammoniumbromide (CTAB, 98%), meso-2,3-Dimercaptosuccinic acid (DMSA, ~98%), ethyl acetate (⩾99.7%) and poly(sodium 4-styrenesulfonate) solution (PSS, 30 wt. % in water). Milli-Q grade water and acetone (>99%) were used as solvents. Standard papers 'Coral' and 'Conqueror' were purchased from Antalis Iberia S.A. and 'Creator Silk' paper was purchased from Torraspapel S.A.

2.2. Nanoparticle synthesis and ink formulation

Ag nanoparticles were prepared following the procedure described by Jiang *et al* [30] with slight variations. In a typical procedure, 2.4 g of PVP was dissolved in 20 ml of ethylene glycol and 0.158 g of $AgNO_3$ was added under magnetic stirring until a yellow color, characteristic of a nano-seed dispersion, was observed. Then the synthesis took place in a Discover S-class closed vessel microwave digestor (CEM) at 200 W during 23 s. After cooling to room temperature the recuperated solid was separated by centrifugation (21 000 rpm) and re-dispersed in DDI water.

The synthesis of gold nanorods was carried out adapting the protocol described by Pastoriza-Santos *et al* [31]. In a typical synthesis 5 ml of 0.2 M CTAB solution was mixed with 5 ml of 0.5 mM $HAuCl_4$ before adding 0.6 ml of 0.01 M $NaBH_4$ and kept under stirring for 5 min to render gold seeds. Separately, 5 ml of 0.2 M CTAB was added to 0.25 ml of 0.004 M $AgNO_3$ in water at 25 °C and 5.0 ml of 0.001 M $HAuCl_4$ was added. This mixture was stirred for 2 min and then 70 μl of 0.0788 M ascorbic acid was added. In a next step 12 μl of the previously prepared seed solution was added to the latter dispersion. The flask with the reactant mixture was heated in a water bath at 28 °C–29 °C. The resulting gold nanorods were washed twice by centrifugation (14 000 rpm, 10 min). To preserve the stability of the nanrods over time PSS was electrostatically attached on the CTAB-capped nanorods [31]. To do that, a beaker with 40 ml of water, 14 mg of NaCl and 72 μl of PSS was placed in an ultrasonic bath until complete dissolution and then the previously prepared gold nanorods were added drop-wise and kept under magnetic stirring for 3 h. All the excess of unbound PSS was removed by centrifugation.

Metallic nanoparticles were transferred when needed to organic media (acetone) following the protocol reported by Wijaya *et al* [32]. The synthesis of magnetite nanoparticles was carried out following the polyol-based protocol described by Cai *et al* [33] and the surface of those magnetic nanoparticles was covalently grafted with DMSA following the work of Sancho *et al* [34] to be able to transfer the nanoparticles to aqueous media.

Screen printing inks were formulated by adding 80 ml of water-based or oil-based varnishes (Manoukian, Kiian SpA, Italy) to the gold (20 ml of gold nanorods (3.7 mg ml^{-1})) or to the silver (20 ml of silver nanoparticles (6.7 mg ml^{-1})) suspensions in either water or acetone depending on whether the screen printing were carried out in water or in organic base, respectively. Screen printing was carried out using a mesh (90 threads/cm) with a specific design. The formulated inks were forced into the mesh openings by the fill blade and were transferred onto the substrate during the squeegee stroke. MP-AES analysis showed that the silver, gold and iron composition in the inks were 143.34 μg of Ag/ml; 126.14 μg Au/ml and 5.25 mg Fe/ml.

2.3. Accelerated aging experiments

To analyze the stability of the nano-based printings over time two accelerated aging tests were performed. An Atlas SUNTEST XXL+ xenon flatbed chamber was used to analyze the weathering effects under Xenon irradiation following the conditions set by the norm UNE-EN ISO 4892-2:2014. A Feutron climatic simulation-test chamber was used to simulate various extreme temperature and humidity environments. Seven consecutive cycles (1 cycle/day) of the following conditions were employed: 5 h at 23 °C ± 3 °C and 90% ± 5% RH; 7 h at 60 °C ± 3 °C and 90% ± 5% RH; 5 h at

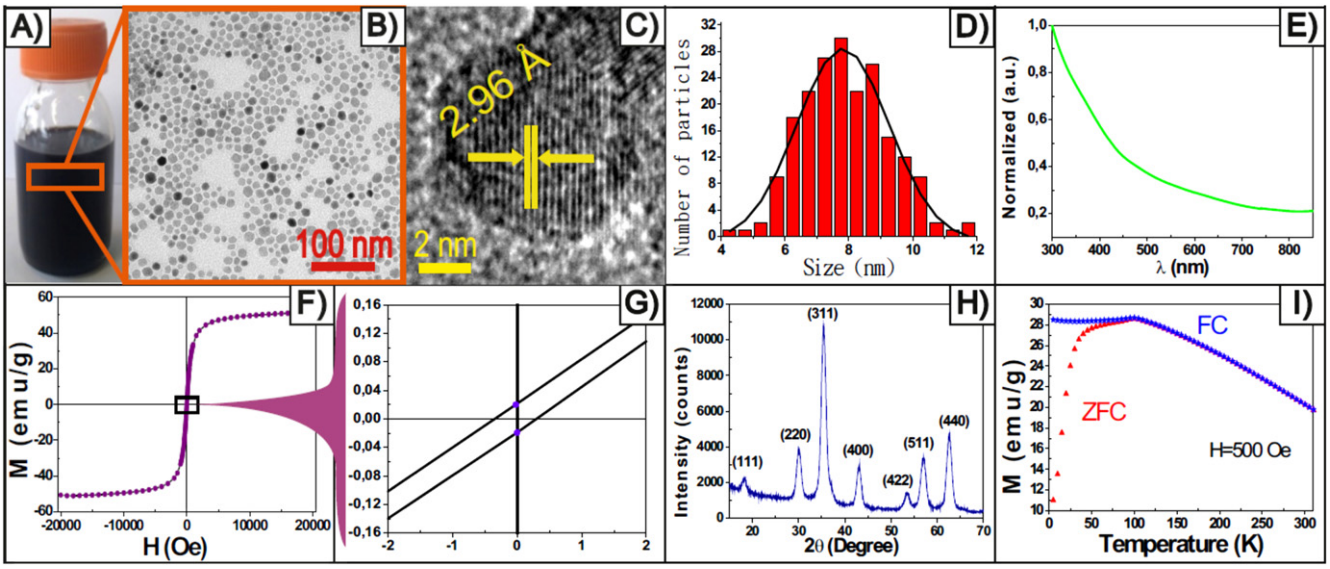

Figure 1. Magnetic nanoparticles produced as anti-counterfeiting nanotaggants. (A) Optical image of the magnetite colloidal dispersion in TEG. (B) Transmission electron micrograph showing the morphology of the nanoparticles. (C) HRTEM photograph of a nanoparticle with interplanar spacing showing the high crystallinity. (D) Histogram of the particle-size distribution. (E) Extinction spectrum of the colloidal magnetite nanoparticles. (F) The magnetization hysteresis loop of produced magnetic nanoparticles. (G) Magnified area of the magnetization hysteresis loop to show the superparamagnetic properties. (H) XRD plot for the Fe_3O_4-DMSA dried sample. (I) ZFC/FC plot at 500 Oe for the Fe_3O_4-DMSA nanoparticles as dried powders.

23 °C ± 3 °C and 90% ± 5% RH; 7 h at -10 °C ± 3 °C and finally the samples were taken at room temperature.

2.4. Characterization of colloidal nanoparticles and nano-based printings

UV–vis extinction spectra of the resulting colloids and printed papers were measured using a UV–vis double beam spectrophotometer Jasco V-670 provided with a holder for solid samples and an integrating sphere. Transmission electron microscopy, TEM, (FEI Tecnai F30 microscope at LMA INA-UNIZAR) was used to examine the morphology of the synthesized nanoparticles. The appearance and distribution of the nanoparticles printed on different types of papers was investigated by scanning electron microscopy, SEM, Quanta FEG-250 by FEI. Silver, gold and magnetite nanoparticle-size distributions in the colloidal dispersions were determined statistically from the TEM micrographs using the National Instruments IMAQ Vision Builder software (N = 100–200 nanoparticles). The crystalline phases in Fe_3O_4-DMSA was evaluated by using an x-ray powder diffractometer (XRD, Rigaku D-Max/2500, Cu Kα radiation source, $\lambda = 0.154\,178$ nm). The XRD pattern was recorded between 15° to 70° (2θ) at $0.3°\,\text{min}^{-1}$. Magnetic properties were analyzed using a vibrating sample magnometer (VSM, Lake Shore 7410) operating at room temperature and 2 Tesla and also in a superconducting quantum interference device (SQUID MPMS-5S, Quantum Design) operating from 0 to 40 000 Oe and at variable temperatures. In the latter case, the samples were measured in a gelatin capsule (a diamagnetic correction for the sample holder was carried out). The temperature dependence of the magnetization was also measured. By means of zero-field-cooled (ZFC) and field-cooled (FC) analysis we obtained the blocking temperature of each sample (the maximum of the ZFC curve), above which the particles are superparamagnetic. The size distribution of the superparamagnetic magnetite nanoparticles was also determined from the measured magnetization curves fitted by a Pseudo-Voigt function based on the Langevin equation. A magnetic pattern recognition sensor (model BS05C by Murata) was used as a magnetic ink document reader. X-ray photoelectron spectroscopy analysis (XPS) was performed with an Axis Ultra DLD (Kratos Tech.). The spectra were excited by the monochromatized AlKα source (1486.6 e.V) run at 15 kV and 10 mA. Analyses of the peaks were performed with the CasaXPS software, using a weighted sum of Lorentzian and Gaussian component curves after background subtraction. The binding energies were referenced to the internal C 1s (284.9 eV) standard. A microwave plasma-atomic emission spectrometer (4100 MP-AES, Agilent Technologies) was used to evaluate the atomic composition of the corresponding samples.

3. Results and discussion

3.1. Magnetic-response nanoparticles

The main characteristics of the magnetite nanoparticles prepared in this work are given in figure 1. The good hydrodynamic stability of the as-prepared magnetite nanoparticles can be appreciated in the optical image of their colloidal dispersion in TEG given in figure 1(A). The good dispersion of the nanoparticles is kept after ligand exchange with

DMSA, as shown in figure 1(B) (a TEM view of the dispersion of Fe_3O_4-DMSA nanoparticles in water). The high-resolution TEM photograph of figure 1(C) allows to appreciate the high crystallinity of the nanoparticles, with lattice fringe spacing of 2.96 Å, very close to the d value for cubic Fe_3O_4 [220] planes (2.97 Å) [35], and figure 1(D) shows the particle-size distribution obtained from TEM observations, which is centered at 7.9 ± 1.4 nm. Figure 1(E) presents the characteristic extinction spectrum of the magnetite nanoparticles where it can be seen that, due to their black color, the nanoparticles absorb in the entire spectrum with increased dispersion observed at lower wavelengths. Figure 1(F) shows the magnetization hysteresis loop of the nanoparticles as dry powder measured with the VSM at 25 °C and 2 Tesla. The area around the origin is shown in detail in figure 1(G). It must be noted that magnetization values are given per unit of total mass (emu/g), considering the total mass of both magnetite nanoparticle and capping agent. The nanoparticles show superparamagnetic behavior with a magnetic moment of 52 emu g^{-1} at 2 Tesla and a coercivity of only 1.3 Oe. The measured magnetization is lower than the magnetic moment reported for pure bulk magnetite samples (92 emu g^{-1}). This is attributed not only to the presence of the capping agent on the surface of the magnetite nanoparticles (which adds to the total sample weight) but also to the increased disorder at the particle surfaces as their size is decreased [36]. MP-AES analysis revealed an iron content in the nanoparticles of 43 wt%. The XRD plot for the dried Fe_3O_4-DMSA sample in figure 1(H) shows the characteristic diffraction peaks matching the cubic inverse spinel of magnetite according to the JCPDS database (file, No. 19-0629). Finally, figure 1(I) shows the ZFC/FC plot at 500 Oe for the Fe_3O_4-DMSA nanoparticles as dried powders with a characteristic blocking temperature at 100 K which indicates a transition from a magnetically blocked state (at low temperature) to a superparamagnetic state (at high temperature). From the hysteresis cycle a Langevin function fitting can be applied to obtain the magnetic crystal size. The value obtained was (7.5 ± 1.1 nm), in good agreement with the particle size measured by TEM. This indicates that monodomain magnetic nanoparticles have been synthesized, and also that interactions between particles are negligible, a basic assumption of the Langevin function. For anti-counterfeiting purposes it is important to note that from the hysteresis loops the particle size can be obtained, potentially a useful parameter for authentication purposes. The simultaneous requirements of a narrow particle-size distribution that yields a unique magnetic signal, and the required surface chemistry to assure colloidal stability over time represent significant challenges for potential forgers.

3.2. Optical-response nanoparticles

Figure 2(A) shows a characteristic TEM micrograph of the produced Ag nanoparticles (an inset with higher magnification is included). Spherical nanoparticles were produced without aggregation, and with a narrow size distribution. The fine control on nanoparticle size is also evidenced by the

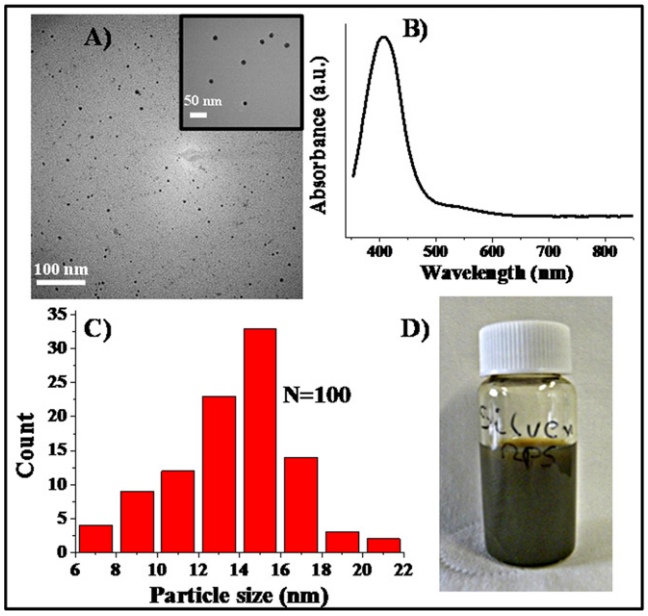

Figure 2. Silver nanoparticle characterization. (A) TEM micrograph showing the morphology of the Ag nanoparticles. (B) UV–vis extinction spectra showing the plasmon resonance peak of silver nanoparticles. (C) Particle-size distribution histogram of silver nanoparticles (15 ± 7 nm). (D) Optical image of the Ag colloidal dispersion in water.

sharp plasmonic resonance peak at 408 ± 3 nm (N = 4) of Ag colloid with a concentration of only 0.039 mg ml^{-1} (figure 2(B)). Figure 2(C) shows the histogram with the particle-size distribution centered at 15 nm. Ag colloidal dispersions in water exhibit a yellowish brown colour due to the excitation of the surface plasmon vibrations (figure 2(D)).

Anisotropic growth of gold in the shape of rods was achieved by a seed-mediated growth, using the selective capping of the [100] facets. Figure 3(A) shows a characteristic TEM micrograph of the Au nanorods, where a highly selective growth to rods as well as a homogenous aspect ratio can be observed (an inset with higher magnification is included). Figure 3(B) depicts the UV–vis extinction spectra of the Au colloids in water (0.022 mg ml^{-1}) showing both transverse (535 ± 3 nm) and longitudinal (762 ± 8 nm; N = 4) surface plasmon resonances. Figures 3(C) and (D) show the histograms with the particle-size distribution centered at 43 and 15.5 nm for the longitudinal and transversal axis of the rods, respectively. The colour of the gold nanorod colloid was reddish-purple, which is the characteristic colour of gold anisotropic nanoparticles adsorbing at 800 nm (figure 3(E)). The plasmon resonance in nanoparticles typically leads to absorption coefficients that are orders of magnitude larger than those of strongly absorbing dyes, and plasmon resonance absorption for anisotropic shapes is even stronger [37]. Therefore, thanks to their stability over time, narrow absorption peaks, and high absorption coefficients, we can conclude that plasmonic nanoparticles present a high potential as taggants offering an attractive alternative to existing technologies.

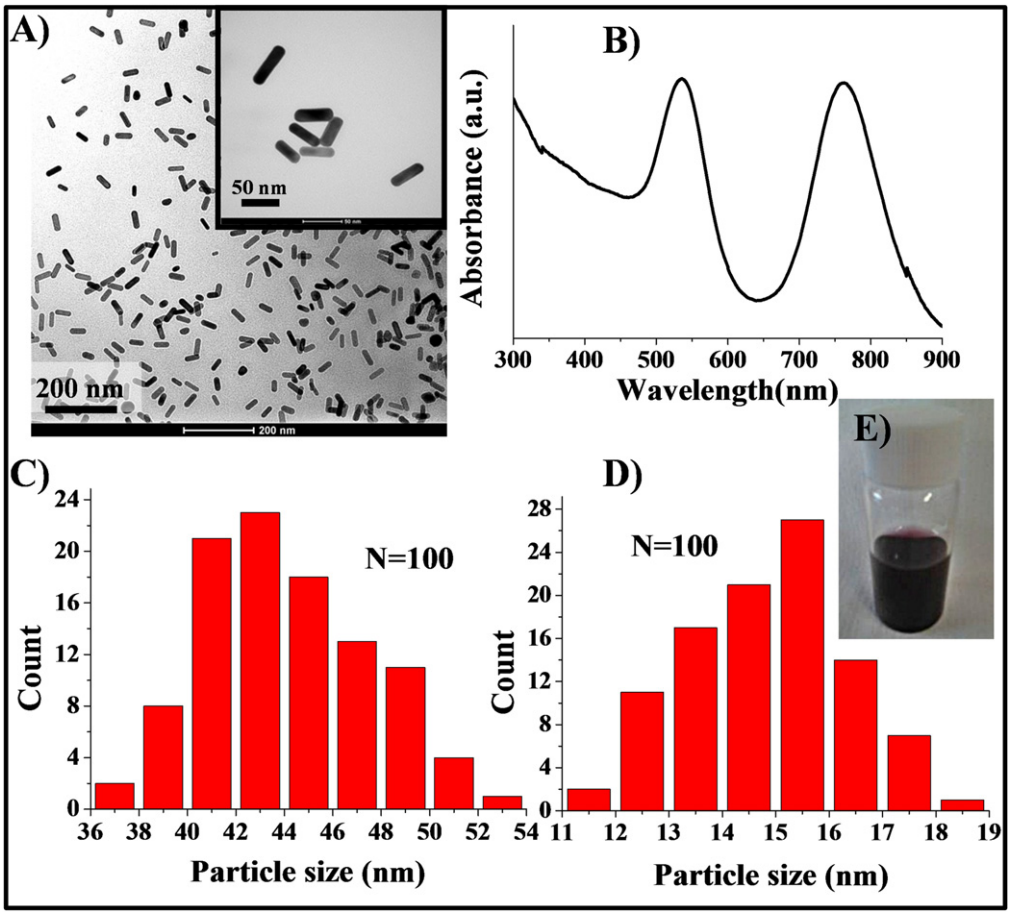

Figure 3. Au nanoparticle characterization. (A) TEM micrograph of as-made Au nanorods (an inset with higher magnification is included). (B) UV–vis extinction spectra of the Au colloids in water. (C) and (D) Histograms with the particle-size distribution for the longitudinal and transversal axis of the rods, respectively. (E) Optical image of the Au nanorod colloidal dispersion in water.

3.3. Nanoparticles as tags on paper supports

The aggregation of nanoparticles and their penetration into the paper used as support were investigated by SEM. Representative images for the printed Ag and Au nanoparticles are depicted in figure 4 where a random distribution of the nanoparticles across the cross-section is clearly observed.

The nanoparticles permeated throughout the (Coral) paper used as support (90 micron thick; figure 4(A)) and could be identified by EDX analysis throughout the cross-section (figures 4(B)–(D)). Figure 4(D) shows the elemental analysis of the section showed in figure 4(C); where Ag was clearly detected together with C and O, coming from the cellulosic fibers, and Si, Al and Ca used as additives and fillers (i.e., SiO_2) during the paper manufacturing process. Figure 4(E) shows the top view of a Coral paper printed with Au-based inks and in figure 4(F) the presence of Au nanoparticles is clearly visible. The same high permeability was observed for magnetite nanoparticles (results not shown) and again iron was detected across the section of the printed paper. This is due to the high porosity of the paper, with pore-sizes much larger than the nanoparticles, facilitating the penetration of the colloidal inks throughout the paper and their consequent bonding to the cellulosic fibers. He *et al* [38] showed that the ether oxygen and the hydroxyl groups anchor metal ions tightly in cellulose fibers via ion−dipole interactions and also stabilize metal nanoparticles by strong bonding interactions with their surface atoms. To corroborate those findings we sonicated (50/60 Hz, 110 W) the printed papers (pieces of 1 cm^2 in 2 ml of water) for 10 min and evaluated the amount of Ag, Au and Fe released from them by using UV–vis or magnetometry (for the Fe_3O_4-DMSA printed samples). We observed that the filtered supernatants were free of nanoparticles, while bundles of broken fibers still contained the nanoparticles attached to them. The metal concentrations on those supernatants were below the detection limit of the UV–vis system.

XPS was also used to corroborate the presence of Fe nanoparticles through the cross-section of the paper. XPS is a surface technique and therefore is limited to characterize the composition of the printed samples in the first few nanometers. However, by using ion etching we were able to analyze the interior of the printed papers beneath the first atomic layers. Also, its high sensitivity (down to ppm) allowed us to corroborate the presence of the Fe nanoparticles on the samples. We observed that the amount of Fe was approximately constant (2.5 ± 0.6 at%) even after 40 min of

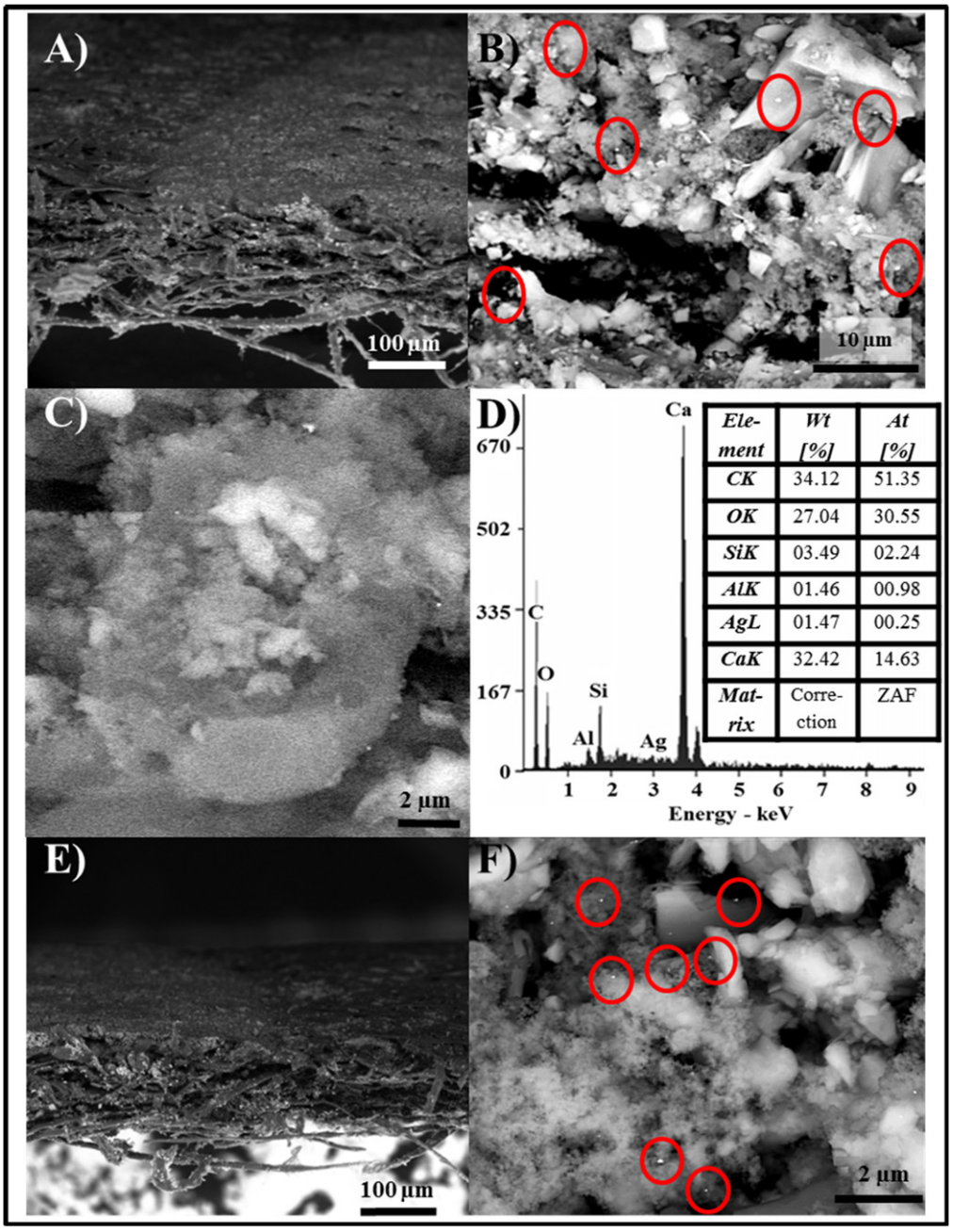

Figure 4. Printed Au and Ag nanoparticles SEM micrographs of (A) top view Coral paper printed with Ag-based inks; (B) and (C) cross-sections of the same paper; (D) EDS analysis of the marked area; (E) top view Coral paper printed with Au-based inks; (F) cross-section of the same paper. The nanoparticle locations are indicated to facilitate identification.

ion etching on the paper surface indicating that the magnetic nanoparticles distribute homogeneously along the cross-section of the printed papers.

The UV–vis spectra of different papers screen printed with Ag-based transparent inks were measured and compared to the response when the same pattern was printed with ink without silver. In figure 5 the characteristic pattern corresponding to the surface plasmon resonance (LSPR) of silver is clearly present, superimposed on the ink + paper response of the circular 5 mm diameter printed patterns. Figures 5(A)–(C) show the characteristic Ag absorption peaks when printing on Creator Silk paper, Coral paper and Conqueror paper, respectively. Blue curves represent the background spectra retrieved from the transparent inks without nanoparticles. As it can be seen, this LSPR induces a strong absorption of the incident light. A maximum of the absorption peak was observed at 444 ± 3 nm, 437 ± 2 nm and 467 nm ± 4 nm depending if the substrate was Creator Silk, Coral or Conqueror, respectively ($N = 4$). Obviously the signals represent the averaged signals provided by the individual nanoparticles randomly deposited on the corresponding substrates. Therefore, the plasmon peak depends on the dielectric nature of the substrate and slight variations on it produced measurable shifts, which could also be used with anti-counterfeiting purposes to validate the papers used as supports. Finally, figure 5(D) shows a photograph of the Ag screen printed

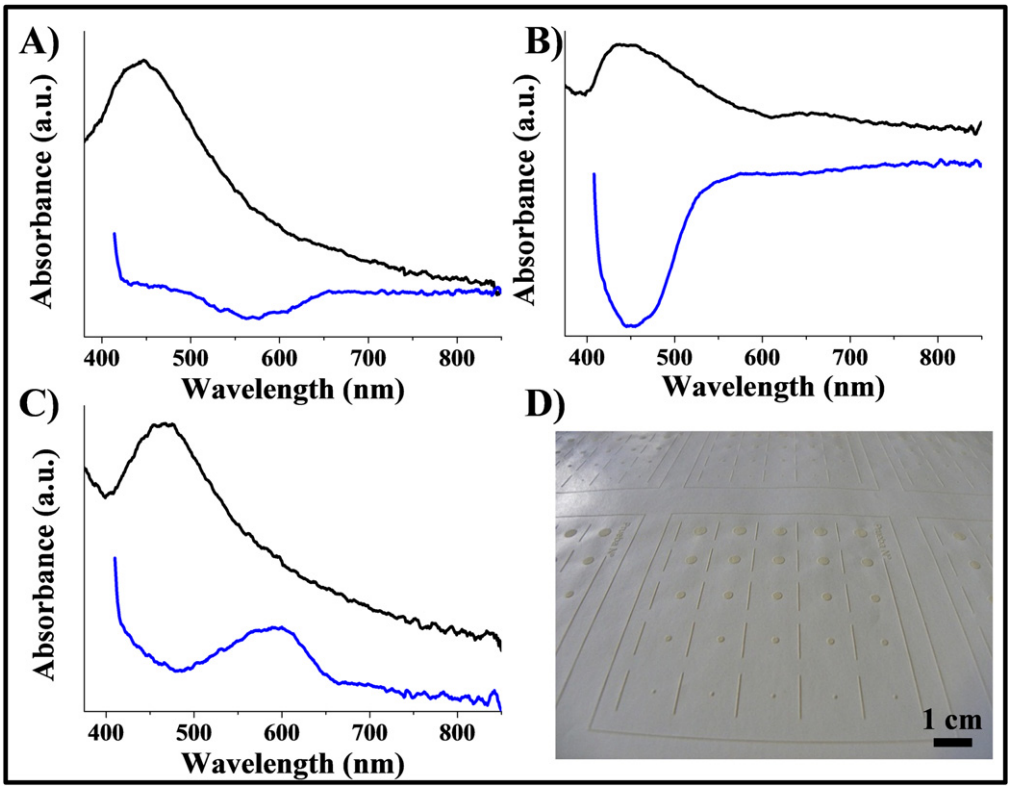

Figure 5. Black curves: UV–vis spectra of silver nanoparticles formulated in transparent ink screen printed as 5 mm diameter circles on the surface of (A) Creator Silk paper, (B) Coral paper and (C) Conqueror paper. Blue curves: background spectra retrieved from the transparent inks without nanoparticles. (D) Digital image of the patterns screen printed on Coral paper.

sample on Coral paper. Although this was the type of paper where a better contrast was obtained, the pattern is rather faint, due to the transparent ink and the low nanoparticle concentration used. In any case, the picture definition is enough to show that, in spite of the presence of nanoparticles a good printing quality can be obtained.

When using gold nanorod-containing transparent inks the color of the printed samples was even fainter compared to the Ag-based printings due to the color of the resulting Au-based inks and the different concentrations used. Figures 6(A)–(C) show the characteristic Au absorption peaks when printing on Creator Silk paper, Coral paper and Conqueror paper, respectively. The characteristic longitudinal and transversal surface plasmon peaks were again dependent on the nature of the substrate. The signal to noise ratio in this case was lower compared with the case of silver-based printings. However, still clear maxima at 519 ± 4 nm and 709 ± 16 nm were measured for the samples printed on Creator Silk paper; at 510 ± 2 nm and 696 ± 11 nm for the samples printed on Coral paper and at 529 ± 2 nm and 697 ± 6 nm ($N = 4$) for the samples printed on Conqueror paper, respectively.

Again, the localized LSPR of metallic nanoparticles depends on the changes in the dielectric constant of the medium and therefore those shifts can be attributed to the different nature of the papers. Compared to the plasmon peaks of the colloidal silver (figure 2(B)), the printed samples show a red shift in the three cases studied, probably due to the nanoparticles agglomeration on the supports. Increasing particle size red shifts the SPR wavelength and also increases the intensity. In the case of gold nanorods a broadening in the plasmon peaks is obvious which is attributed to contributions from higher order electron oscillations [39]. In spite of this broadening characteristic of the printed samples, the signal to noise ratio is well above the levels needed for identification of the maximum peaks and therefore authentication of the signals is feasible. If needed, the signal to noise ratio can be further increased by increasing the nanoparticle concentration in the ink, or by increasing the number of print runs.

The magnetic signals of these printed circular samples (5 mm in diameter) were also collected using VSM (figure 7). Figure 7(A) shows that an increased number of printings on Coral paper produces, as expected, an increase in the intensity of the signal collected due to the higher density of the superparamagnetic nanoparticles present in the sample. Independent measurements of the magnetic signals provided by 4 independent printings showed a saturation magnetization of 675 ± 15 μemu and 1532 ± 72 μemu for samples printed once and twice, respectively. Figure 7(B) shows the responses obtained from printings on different types of paper. It can be seen that the influence of the nature of the support is weak for the three types of paper tested. Different types of paper have different porosities and surface groups on the paper fibers. This means that the spatial distribution of nanoparticles can be very different (as, for instance, more porous and hydrophilic papers will enable a deeper and wider penetration of

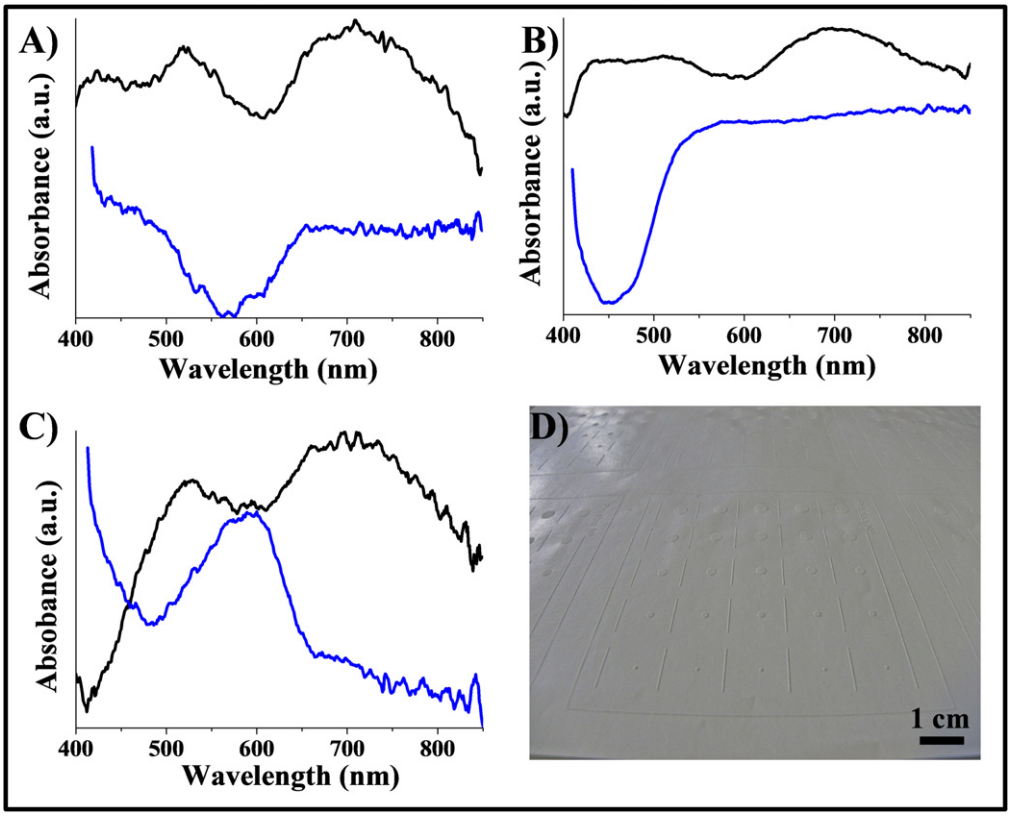

Figure 6. Black curves: UV–vis spectra of the gold nanorods formulated in transparent ink screen printed as 5 mm diameter circles on the surface on the surface of (A) Creator Silk paper, (B) Coral paper and (C) Conqueror paper. Blue curves: background spectra retrieved from the transparent inks without nanoparticles. (D) Digital image of the patterns screen printed on Coral paper.

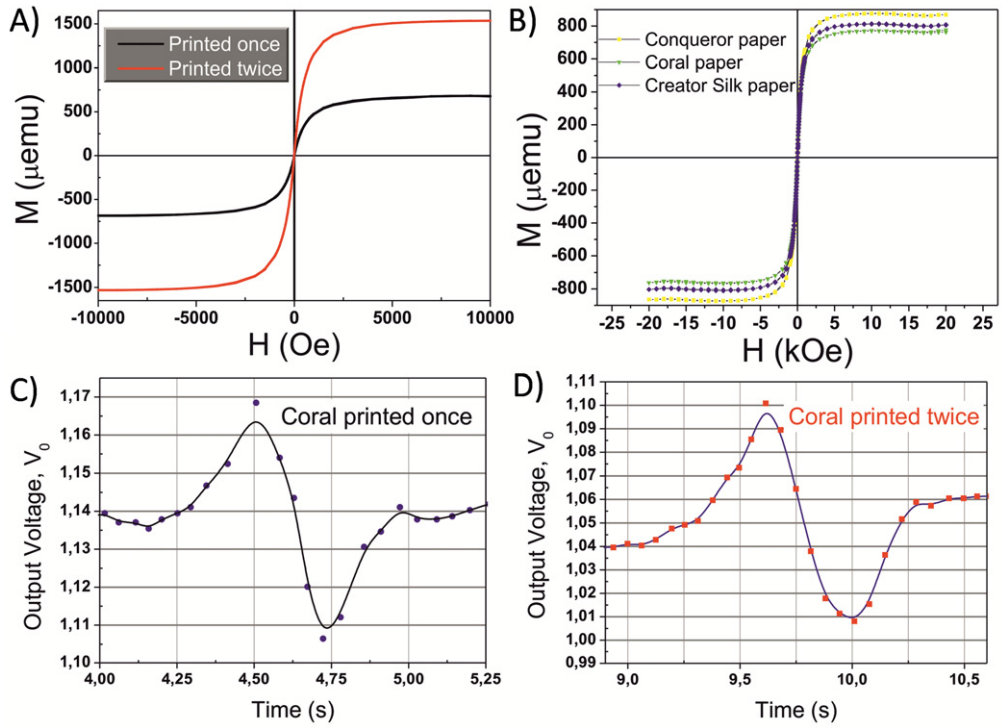

Figure 7. Magnetization curves of the different screen printed samples (spots 5 mm in diameter) using Fe_3O_4-DMSA based inks: (A) the amount of magnetic materials deposited and consequently the magnetic signal increase with the number of strokes during the screen printing process. (B) Magnetization curves of the same Fe_3O_4-DMSA ink on different papers. (C) Output voltage retrieved from the commercial magnetic pattern recognition sensor after scanning the (1 time) printed paper (variation of the signal = 0.05 vol). (D) Output voltage retrieved from the magnetic pattern recognition sensor after scanning the (2 times) printed paper (variation of the signal = 0.09 vol).

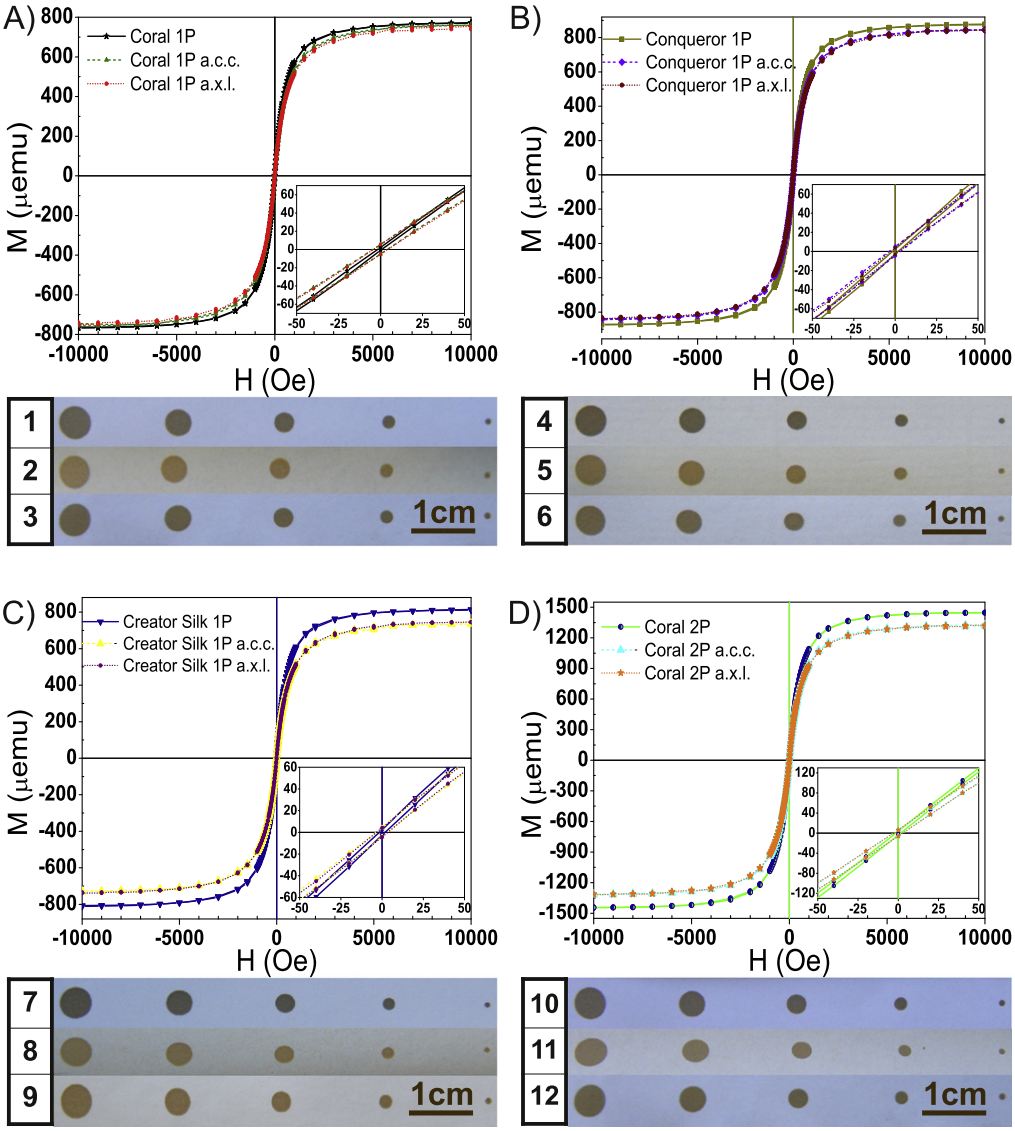

Figure 8. Hysteresis loops of the magnetite-based inks printed on different supports. The zoom as an inset shows the region close to the origin to show the coercive field. (A) Coral paper, after one print run and after being subjected to climatic chamber (a.c.c.) and Xe irradiation (a.x.l.). (B) Conqueror paper, same nomenclature. (C) Creator Silk paper, same nomenclature. (D) Coral paper, same as (A), but after two print runs. 1–12: photographs of circular patterns screen printed with magnetic ink: from left to right the size decreases from 5 mm to 1 mm diameter. Coral paper, (1) after being printed, (2) after Xe irradiation (3) after climatic chamber, respectively. (4–6) Same for Conqueror paper; (7–9) Same for Creator Silk paper; (10–12) Same for Coral paper (printed twice).

water-based inks into the support). These influences translate into a strong dependence of the optical response on the support characteristics. Thus, as we have seen, the type of paper has a strong influence on the signals obtained from Ag and Au-containing inks (figures 5 and 6), since those nanoparticles sitting deeper into the support will have a strongly diminished contribution to the optical response. The case with magnetic response is different, as seen in figure 7(B). The penetration of the magnetic field is much higher than the sample depth, and therefore all nanoparticles contribute, independently of their location. Finally, figures 7(C) and (D) show the electrical response retrieved after scanning a printed spot (4 mm) with the commercial magnetic pattern recognition sensor (samples printed once (figure 7(C)) and twice (figure 7(D)) on Coral paper. This sensor provides an output voltage independent of the scanning speed and an easily measured signal was observed which increased depending on the amount deposited.

By cutting out and digesting 5 mm diameter printed spots, the amount of iron was evaluated as 0.3 μg Fe mm^{-2} (the amounts obtained for Ag and Au over the same surface area were 0.001 μg Ag mm^{-2} and 0.0037 μg Au mm^{-2}). The main advantage of using superparamagnetic nanoparticles compared to ferromagnetic ones is that the latter tend to agglomerate due to their permanent magnetic dipoles and therefore superparamagnetic nanoparticles are a good choice for preparing inks that are stable over time. We observed that the magnetite colloids and the prepared inks in both organic and aqueous media were stable in storage for six months without showing any sedimentation.

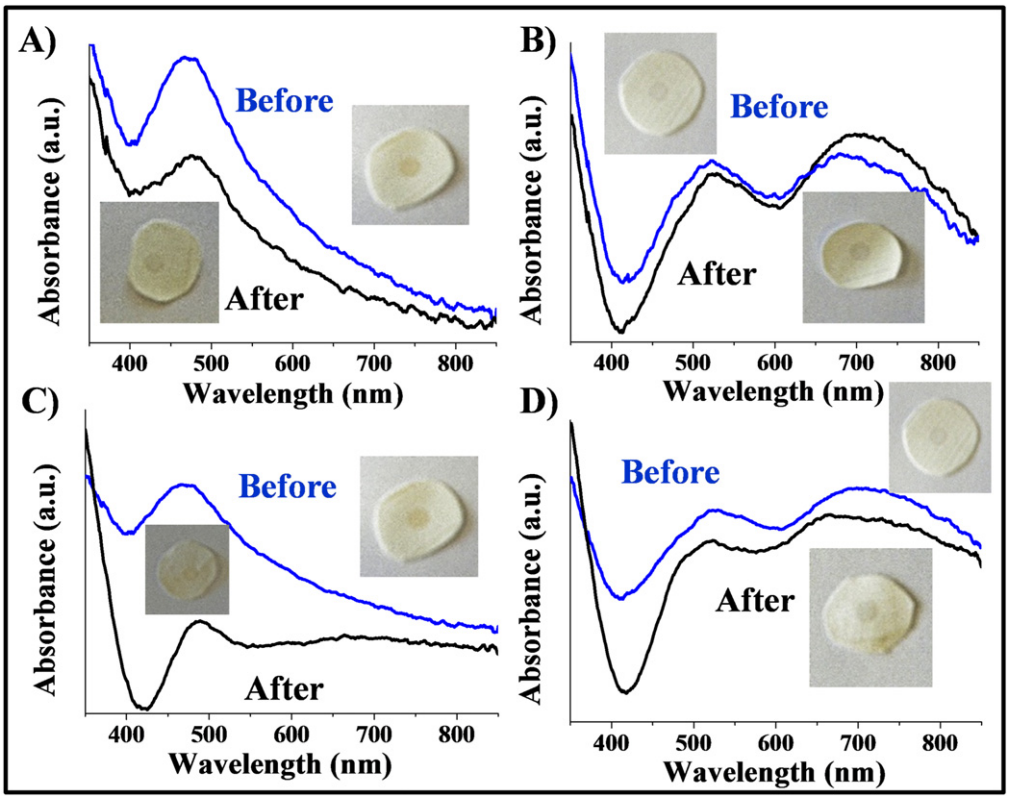

Figure 9. UV–vis spectra collected for silver nanoparticles before and after the accelerated atmospheric weathering test (A) and the xenon irradiation test (C). UV–vis spectra collected for gold nanorods before and after the accelerated atmospheric weathering test (B) and the xenon irradiation test (D).

3.4. Effect of aging

The stability of the printed marks with time is an important consideration regarding potential authentication applications. Since it is not possible to wait for the time (possibly years) required to evaluate aging effects under conditions representative of real use, accelerated aging tests were carried out on printed samples using Xe irradiation and severe temperature and humidity cycling, as described in the experimental section. The magnetic response of the different samples after these accelerated weathering procedures is shown in figure 8. It can be seen that aging induced minimal changes in the magnetic response of the printed nanoparticles on the three different papers tested, indicating that magnetic labelling is very resistant to deterioration processes. Visually, slight fading was observed in the appearance of the printed patterns after the tests. In the case of the Xe irradiated samples a slight transition from black (magnetite) to brownish (maghemite) was appreciated, indicating that Xe light accelerates the naturally occurring process of oxidation from magnetite to maghemite.

Tang *et al* [40] showed that visible light does not have any influence in the transformation from magnetite to maghemite but UV light (100 to 400 nm) does. The xenon lamp used in the tests emits photons starting at 300 nm. In fact, figure 8 shows a slight reduction in the magnetic signal after accelerated aging, being more pronounced the effect of the xenon irradiation. A maximum reduction in the magnetic moment of only 4.7, 3.3, 7.7 and 9.4% in the signals was measured for the samples printed on Coral (figure 8(A)), Conqueror (figure 8(B)), Creator Silk (figure 8(C)) and Coral (printed twice; figure 8(D)) respectively. Still, after aging the magnetic detection was unaltered using the magnetic pattern recognition sensor, indicating the robustness of the magnetic nanoparticles as taggants. Unrelated to the magnetic tagging, it can be observed that the xenon irradiation darkened all the papers. The photo-degradation of cellulose was studied by Malešič *et al* [41] who concluded that exposure at wavelengths above 340 nm produces oxidative degradation accompanied by formation of hydroxyl radicals and carbonyl groups.

Figure 9 shows the accelerated weathering results for the printings based on gold (figures 9(B) and (D)) and silver (figures 9(A) and (C)) nanoparticles using UV–vis spectrometry. The extinction spectra decreased significantly compared to the original samples and that reduction was more pronounced for silver printings than for gold printings. The oxidative effect was more noticeable when the samples were exposed to the xenon irradiating lamp. It is well known that silver can be photo-oxidized forming a passivation silver oxide layer around the metallic cores [42]. The water present in the humid weathering atmosphere plays also an important role in the oxidation of the silver nanoparticles. Lok *et al* [43] demonstrated that silver nanoparticles obtained by reduction and prevented from further oxidation did not show any bactericidal effects (release of ionic silver) whereas those

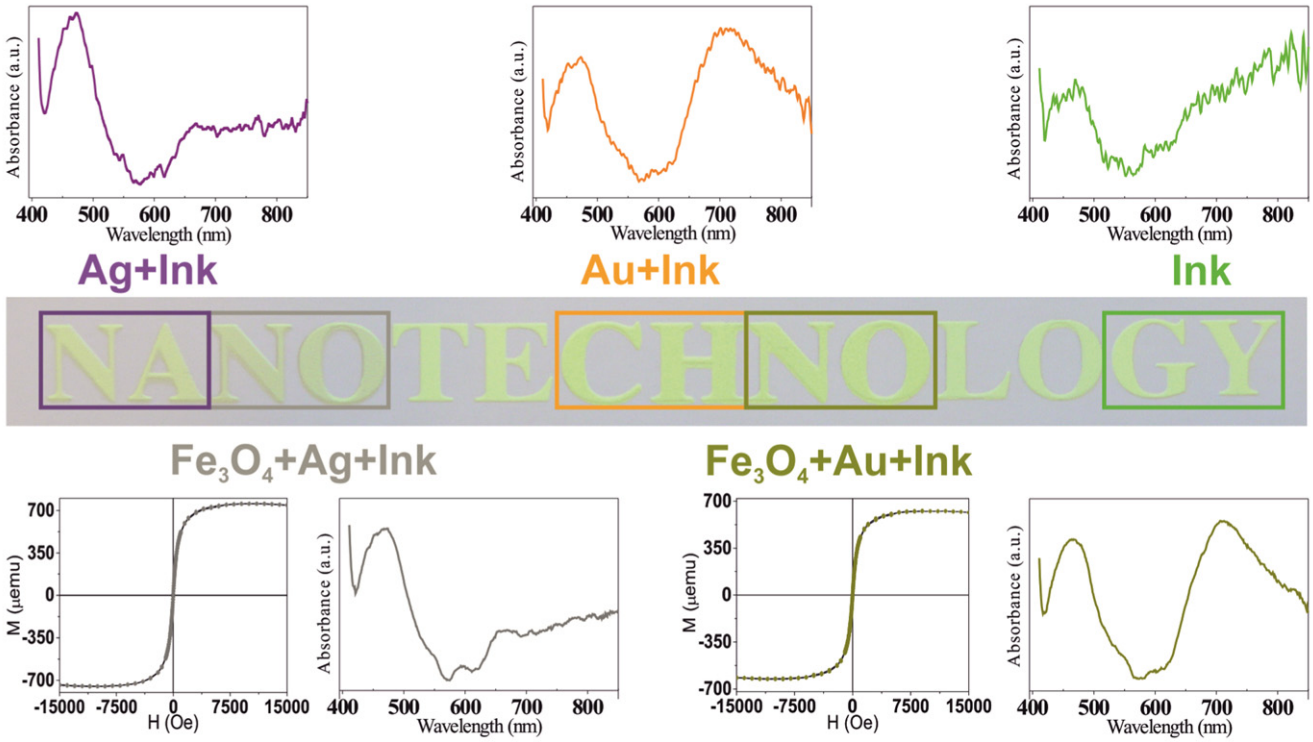

Figure 10. Digital image of a printing on Coated Creator paper showing the word '*Nanotechnology*' in which the letters 'NA' have been screen printed with Ag nanoparticles, the letters 'CH' with gold nanorods, the letters 'GY' with commercial green ink (as well as all of them), the first letters 'NO' have two overlapping layers, the first printed with magnetic nanoparticles and on top of it the same printing with Ag nanoparticles; the second letters 'NO' also contain two overlapping layers, the one underneath printed with magnetic nanoparticles and the one on top printed with gold nanorods.

nanoparticles partially oxidized showed a strong bactericidal action. Therefore water plays an important role in the redox reaction to form oxidized silver. The redshift observed in the extinction spectra of the silver printed samples is also an indication that silver oxide was formed [43]. Still, the optical signals characteristic of Ag nanoparticles and Au nanorods are clearly present in the aged samples, indicating that the tags can successfully survive severe aging tests.

Finally, the combination of different anti-counterfeiting tags is desirable because it increases the level of protection, as discussed in the introduction. Magnetic and optical signals can be used independently, as in the examples discussed above, or combined, using separate letters on the same encrypted text. In addition, they can be combined on the same printed letters by using overlapping printings of both magnetic and optical (silver and/or gold) inks. In addition, the nanoparticles used as tags printed on paper must be able to provide signals that are considerably more intense than those of the inks used. An illustrative example is given in figure 10, where a template with different printings (the word '*Nanotechnology*') has been printed with green ink on Coated Creator paper. In this case some letters have been printed with one (or no) tags, while others have been printed with the magnetic nanoparticle-based inks and re-printed in a second screen printing process with gold or silver-based inks. The results indicate that the labeling signals can be obtained with excellent quality, either alone or in combination with other tags.

Comparing all the results we demonstrate the high colloidal stability of magnetic and gold nanoparticles after dispersing them in different inks and after printing them on different supports even when using accelerated weathering conditions. Also the photo-stability of silver nanoparticles can be enhanced when protected into the cellulosic fibers.

4. Conclusions

Screen printing is suitable for printing inks containing magnetic and plasmonic nanoparticles. A good printing quality can be obtained on different substrates and their physical signals are easily obtained, even when in combinations of optical and magnetic-response tags. The printed signals are sufficiently stable under accelerated weathering conditions, an important advantage over the usual response of conventional chromophores, which are more prone to signal fading under light or humidity. The nanoparticle surface functionalization with PVP (on Ag), PSS (on Au) and DMSA (on Fe_3O_4) favors their colloidal stability in aqueous media when formulating serigraphy inks. In organic media dodecanethiol (on Ag and Au) and TEG (on Fe_3O_4) provide the resulting nanoparticles with colloidal stability when formulated as inks. The reduced nanoparticle size also makes nanoparticle-loaded inks permeable throughout paper-based supports which can also be advantageous due to the protective action of the cellulosic fibers. Finally, the well-known surface

chemistry of magnetic and plasmonic nanoparticles enables easy transfer to a variety of both organic and polar solvents enabling multiple printing applications.

Acknowledgment

We are especially grateful to Pepe Bofarull for his invaluable help and guidance during the screen printing process. Financial support from Tipolínea SAU, from the EU thanks to the ERC Consolidator Grant program (ERC-2013-CoG-614715, NANOHEDONISM), the Government of Aragon and the European Social Fund are gratefully acknowledged. CIBER-BBN is an initiative funded by the VI National R&D&i Plan 2008-2011, Iniciativa Ingenio 2010, Consolider Program, CIBER Actions and financed by the Instituto de Salud Carlos III with assistance from the European Regional Development Fund.

References

[1] http://iccwbo.org/products-and-services/fighting-commercial-crime/counterfeiting-intelligence-bureau/ (Accessed 5 May 2015)
[2] Wang L Y and Li Y D 2007 Controlled synthesis and luminescence of lanthanide doped $NaYF_4$ nanocrystals *Chem. Mater.* **19** 727–34
[3] Blumenthal T, Meruga J, May P S, Kellar J, Cross W, Ankireddy K, Vunnam S and Luu Q N 2012 Patterned direct-write and screen-printing of NIR-to-visible upconverting inks for security applications *Nanotechnology* **23** 185305
[4] You M L, Zhong J J, Hong Y, Duan Z F, Lin M and Xu F 2015 Inkjet printing of upconversion nanoparticles for anti-counterfeit applications *Nanoscale* **7** 4423–31
[5] Meruga J M, Cross W M, May P S, Luu Q, Crawford G A and Kellar J J 2012 Security printing of covert quick response codes using upconverting nanoparticle inks *Nanotechnology* **23** 395201
[6] Sangeetha N M, Moutet P, Lagarde D, Sallen G, Urbaszek B, Marie X, Viau G and Ressier L 2013 3D assembly of upconverting NaYF4 nanocrystals by AFM nanoxerography: creation of anti-counterfeiting microtags *Nanoscale* **5** 9587–92
[7] Zhang Y H, Zhang L X, Deng R R, Tian J, Zong Y, Jin D Y and Liu X G 2014 Multicolor barcoding in a single upconversion crystal *J. Am. Chem. Soc.* **136** 4893–6
[8] Zhu L L, Yin Y J, Wang C F and Chen S 2013 Plant leaf-derived fluorescent carbon dots for sensing, patterning and coding *J. Mater. Chem.* C **1** 4925–32
[9] Kshirsagar A, Jiang Z, Pickering S, Xu J and Ruzyllo J 2013 Formation of photo-luminescent patterns on paper using nanocrystalline quantum dot ink and mist deposition *ECS J. Solid State Sc.* **2** R87–90
[10] Kuemin C, Nowack L, Bozano L, Spencer N D and Wolf H 2012 Oriented assembly of gold nanorods on the single-particle level *Adv. Funct. Mater.* **22** 702–8
[11] Kumar P, Dwivedi J and Gupta B K 2014 Highly luminescent dual mode rare-earth nanorod assisted multi-stage excitable security ink for anti-counterfeiting applications *J. Mater. Chem.* C **2** 10468–75
[12] Esenturk E N and Walker A R H 2009 Surface-enhanced Raman scattering spectroscopy via gold nanostars *J. Raman Spectrosc.* **40** 86–91
[13] Cui Y, Hegde R S, Phang I Y, Lee H K and Ling X Y 2014 Encoding molecular information in plasmonic nanostructures for anti-counterfeiting applications *Nanoscale* **6** 282–8
[14] Gaufres E, Tang N Y W, Lapointe F, Cabana J, Nadon M A, Cottenye N, Raymond F, Szkopek T and Martel R 2014 Giant Raman scattering from J-aggregated dyes inside carbon nanotubes for multispectral imaging *Nat. Photonics* **8** 72–8
[15] Pham H H, Gourevich I, Oh J K, Jonkman J E N and Kumacheva E 2004 A multidye nanostructured material for optical data storage and security data encryption *Adv. Mater.* **16** 516
[16] Montelongo Y, Tenorio-Pearl J O, Williams C, Zhang S, Milne W I and Wilkinson T D 2014 Plasmonic nanoparticle scattering for color holograms *Proc. Natl Acad. Sci. USA* **111** 12679–83
[17] Tomita Y, Suzuki N and Chikama K 2005 Holographic manipulation of nanoparticle distribution morphology in nanoparticle-dispersed photopolymers *Opt. Lett.* **30** 839–41
[18] Park K W 2005 Electrochromic properties of Au-WO3 nanocomposite thin-film electrode *Electrochim. Acta* **50** 4690–3
[19] Lee K G, Choi B G, Kim B I, Shyu T, Oh M S, Im S G, Chang S J, Lee T J, Kotov N A and Lee S J 2014 Scalable nanopillar arrays with layer-by-layer patterned overt and covert images *Adv. Mater.* **26** 6119
[20] Yan P, Fei G T, Su Y, Shang G L, Li H, Wu B and Zhang L D 2012 Anti-counterfeiting of one-dimensional alumina photonic crystal by creating defects *Electrochem. Solid St.* **15** K23–6
[21] Sen S 2004 Nanoprinting with nanoparticles: concept of a novel inkjet printer with possible applications in invisible tagging of objects *J. Disper. Sci. Technol.* **25** 523–8
[22] Xuan R Y and Ge J P 2011 Photonic printing through the orientational tuning of photonic structures and its application to anticounterfeiting labels *Langmuir* **27** 5694–9
[23] Hu H B, Chen Q W, Tang J, Hu X Y and Zhou X H 2012 Photonic anti-counterfeiting using structural colors derived from magnetic-responsive photonic crystals with double photonic bandgap heterostructures *J. Mater. Chem.* **22** 11048–53
[24] Puddu M, Paunescu D, Stark W J and Grass R N 2014 Magnetically recoverable, thermostable, hydrophobic DNA/silica encapsulates and their application as invisible oil tags *Acs Nano* **8** 2677–85
[25] Duong B, Liu H L, Ma L Y and Su M 2014 Covert thermal barcodes based on phase change nanoparticles *Sci. Rep.* **4** 5170
[26] Wilcoxon J P and Provencio P P 2004 Heterogeneous growth of metal clusters from solutions of seed nanoparticles *J. Am. Chem. Soc.* **126** 6402–8
[27] Kim J, Yun J M, Jung J, Song H, Kim J B and Ihee H 2014 Anti-counterfeit nanoscale fingerprints based on randomly distributed nanowires *Nanotechnology* **25** 155303
[28] Zhao J P, Wei Z W, Feng X, Miao M, Sun L N, Cao S M, Shi L Y and Fang J H 2014 Luminescent and transparent nanopaper based on rare-earth up-converting nanoparticle grafted nanofibrillated cellulose derived from garlic skin *Acs Appl. Mater. Inter.* **6** 14945–51
[29] Creran B, Yan B, Moyano D F, Gilbert M M, Vachet R W and Rotello V M 2012 Laser desorption ionization mass spectrometric imaging of mass barcoded gold nanoparticles for security applications *Chem. Commun.* **48** 4543–5
[30] Komarneni S, Li D S, Newalkar B, Katsuki H and Bhalla A S 2002 Microwave-polyol process for Pt and Ag nanoparticles *Langmuir* **18** 5959–62

[31] Pastoriza-Santos I, Perez-Juste J and Liz-Marzan L M 2006 Silica-coating and hydrophobation of CTAB-stabilized gold nanorods *Chem. Mater.* **18** 2465–7
[32] Wijaya A and Hamad-Schifferli K 2008 Ligand customization and DNA functionalization of gold nanorods via round-trip phase transfer ligand exchange *Langmuir* **24** 9966–9
[33] Cai W and Wan J Q 2007 Facile synthesis of superparamagnetic magnetite nanoparticles in liquid polyols *J. Colloid Interf. Sci.* **305** 366–70
[34] Miguel-Sancho N, Bomati-Miguel O, Colom G, Salvador J P, Marco M P and Santamaria J 2011 Development of stable, water-dispersible, and biofunctionalizable superparamagnetic iron oxide nanoparticles *Chem. Mater.* **23** 2795–802
[35] Berry L G T R (ed) 1962 *X-Ray Diffraction Data for Minerals* (Baltimore, MD: Waverly)
[36] Shah P, Sohma M, Kawaguchi K and Yamaguchi I 2002 Growth conditions, structural and magnetic properties of M/Fe_3O_4/I (M = Al, Ag and I = Al_2O_3, MgO) multilayers *J. Magn. Magn. Mater.* **247** 1–5
[37] Eustis S and El-Sayed M A 2006 Why gold nanoparticles are more precious than pretty gold: noble metal surface plasmon resonance and its enhancement of the radiative and nonradiative properties of nanocrystals of different shapes *Chem. Soc. Rev.* **35** 209–17
[38] He J H, Kunitake T and Nakao A 2003 Facile in situ synthesis of noble metal nanoparticles in porous cellulose fibers *Chem. Mater.* **15** 4401–6
[39] Huang X and El-Sayed M A 2010 Gold nanoparticles: optical properties and implementations in cancer diagnosis and photothermal therapy *J. Adv. Res.* **1** 13–28
[40] Tang J, Myers M, Bosnick K A and Brus L E 2003 Magnetite Fe_3O_4 nanocrystals: spectroscopic observation of aqueous oxidation kinetics *J. Phys. Chem.* B **107** 7501–6
[41] Malesic J, Kolar J, Strlic M, Kocar D, Fromageot D, Lemaire J and Haillant O 2005 Photo-induced degradation of cellulose *Polym. Degrad. Stabil.* **89** 64–9
[42] Grillet N, Manchon D, Cottancin E, Bertorelle F, Bonnet C, Broyer M, Lerme J and Pellarin M 2013 Photo-oxidation of individual silver nanoparticles: a real-time tracking of optical and morphological changes *J. Phys. Chem.* C **117** 2274–82
[43] Lok C N, Ho C M, Chen R, He Q Y, Yu W Y, Sun H, Tam P K H, Chiu J F and Che C M 2007 Silver nanoparticles: partial oxidation and antibacterial activities *J. Biol. Inorg. Chem.* **12** 527–34